

Finite element analysis of carbon fiber-reinforced polymer (CFRP) strengthened reinforced concrete beams

SangHun Kim[†] and Riyad S. Aboutaha[‡]

*Department of Civil and Environmental Engineering, Syracuse University, Syracuse, NY 13244, U.S.A.
(Received October 11, 2003, Accepted November 10, 2004)*

Abstract. This paper presents investigation of a three-dimensional (3-D) nonlinear finite element model analysis to examine the behavior of reinforced concrete beams strengthened with Carbon Fiber Reinforced Polymer (CFRP) composites to enhance the flexural capacity and ductility of the beams. Three-dimensional nonlinear finite element models were developed between the internal reinforcement and concrete using a smeared relationship. In addition, bond models between the concrete surface and CFRP composite were developed using a smeared bond for general analyses and a contact bond for sensitivity analyses. The results of the FEA were compared with the experimental data on full-scale members. The results of two finite-element bonding models showed good agreement with those of the experimental tests.

Keywords: FEM; CFRP; CFRP anchorage system; flexural strength; ductility; bond; contact.

1. Introduction

CFRP composites are effective materials for strengthening existing reinforced concrete structures. Many researchers have investigated the effects of CFRP composites on behavior of strengthened reinforced concrete beams. However, few researchers have performed numerical analyses on fiber reinforced polymer (FRP) strengthened beams using finite element analysis (FEA) method. Ross, *et al.* (1999) conducted 2-D nonlinear FEA assuming perfect bonding between the concrete and FRP composite. The results of the analyses indicated slightly lower strength than the experimental results. Wong and Vecchio (2003) performed a 2-D nonlinear FEA assuming both perfect bonding and non-perfect bonding models. The results showed good agreement with the experimental results in load-deflection relationships up to the separation of the FRP system from the concrete surface. Kachlakev (2002) performed a 3-D nonlinear FEA assuming perfect bonding between the concrete and FRP composite for shear strengthening. The results of the FEA model showed good agreement with the experimental data.

In this paper, the results of a 3-D nonlinear FEA models utilizing both perfect bonding and non-perfect (contact) bonding elements at the concrete-CFRP interface for flexural strengthening are presented. The FEA results are compared with the experimental results of sixteen full-scale beams for the load-deformation relationship. Furthermore, the FEA results are compared with the experimental and ACI results at the ultimate load.

[†] Research Associate

[‡] Associate Professor

2. Research significance

Over the last decade many researchers have studied retrofitting and rehabilitating reinforced and prestressed concrete structures using FRP composites. Several important design guidelines were suggested such as the practical design guideline provided by the ACI 440 report (2000). In this paper, the FEA models are presented to offer a more detailed and accurate design procedure. In addition CFRP diagonal anchors are also introduced for enhancing the ductility of the strengthened beams.

3. Experimental program

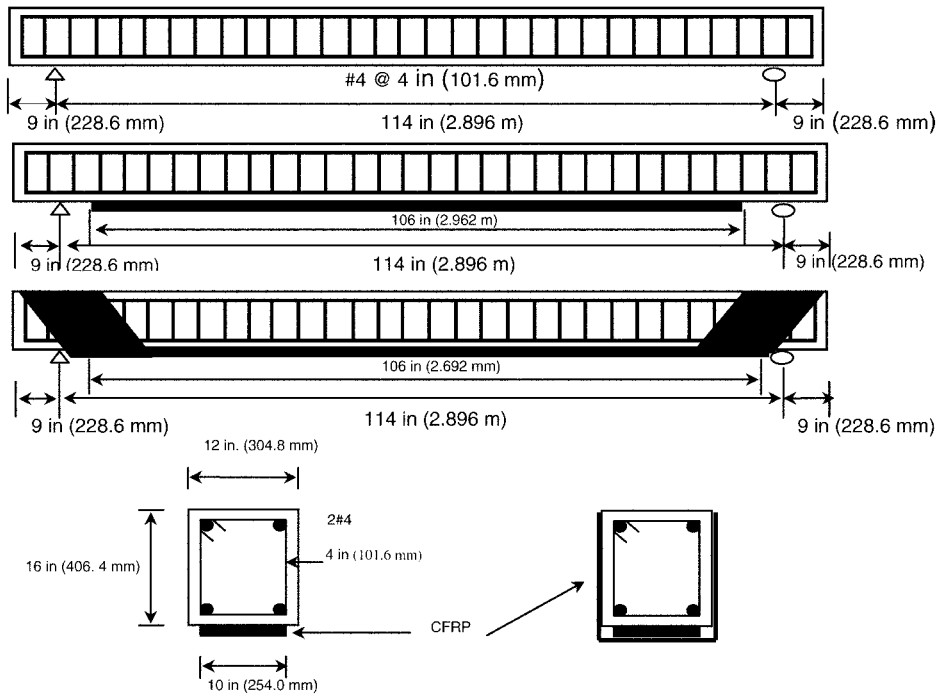
Sixteen full-scale under-reinforced concrete beams were investigated in the Structural Laboratory at Syracuse University. The sixteen beams were divided into four groups. Groups 1 and 2 each consisted of four-rectangular beams and Groups 3 and 4 consisted of four T-beams and six T-beams, respectively. Details of the test beams are summarized in Table 1. Geometries of the beams are shown in Fig. 1. The cross-sections of the rectangular beams were 12 in (304.8 mm) wide by 16 in (406.4 mm) high. The cross-sections of the T-shaped beams were 30 in (762 mm) in flange width, 12 in (304.8 mm) in web width, and 16 in (406.4 mm) in height. The total length of each beam was 11 ft (3352.8 mm) and the span between the supports was 9 ft 6 in (2895.6 mm). The cross section of each unidirectional CFRP composite sheet was 0.0066 inch thick by 10 inch wide (0.168 mm \times 254 mm). Beams were strengthened with either longitudinal CFRP sheets on the tension side or longitudinal CFRP sheets on the tension side along with diagonal CFRP anchors. The diagonal CFRP anchors are made of uniaxial CFRP sheets, the same as the longitudinal CFRP sheets. The advantage of the diagonal CFRP anchors is that they allow clamping of the longitudinal CFRP sheets to prevent premature debonding. In addition, at the bottom of the beam they have two components; in the transverse and longitudinal directions, which allows for better transfer of forces from the CFRP longitudinal sheets to the CFRP diagonal anchors.

The average tensile strength of CFRP composite sheets is given in Table 2. The average concrete compressive strengths were 5250 psi (36.2 MPa) for the rectangular beams in Groups 1 and 2, 4435 psi (30.6 MPa) for the T-shaped beams in Group 3, and 2000 psi (13.8 MPa) for T-shaped beams in Group 4. Grade 60 steel (414 MPa) was used. The actual average tensile yielding strengths of steel rebars varied from 50 to 79 ksi (345 to 545 MPa). Fig. 2 shows the stress-strain properties for concrete and steel.

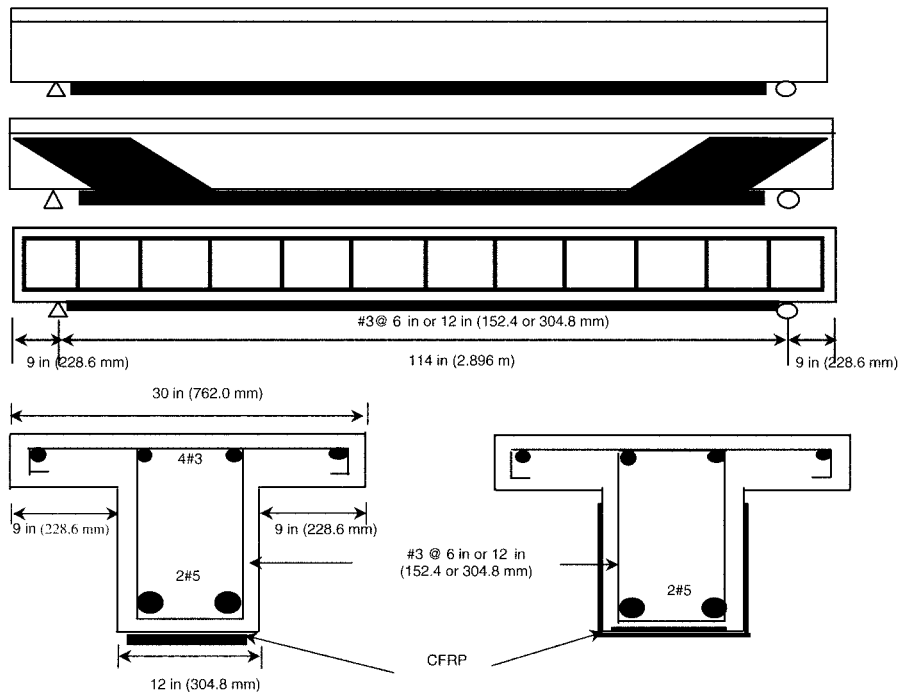
4. Finite element analysis (FEA)

4.1. FEA Models and Elements

A 3-D nonlinear FEA was performed using the commercial FEA program, ANSYS (2002). Two FEA models were used to model the perfect bonding and non-perfect (contact) bonding between the concrete surfaces and the CFRP sheets. The geometrical details of FEA model beams are shown as Figs. 3 and 4. For both models, steel reinforcements were smeared into solid elements with sharing nodes. For the perfect bonding model, CFRP elements were smeared into solid elements, and for the non-perfect bonding model, bonding elements were used for sensitivity analyses.



(a) Rectangular specimens in Groups 1 & 2



(b) T-shape specimens in Groups 3 & 4

Fig. 1 Details of experimental test specimens

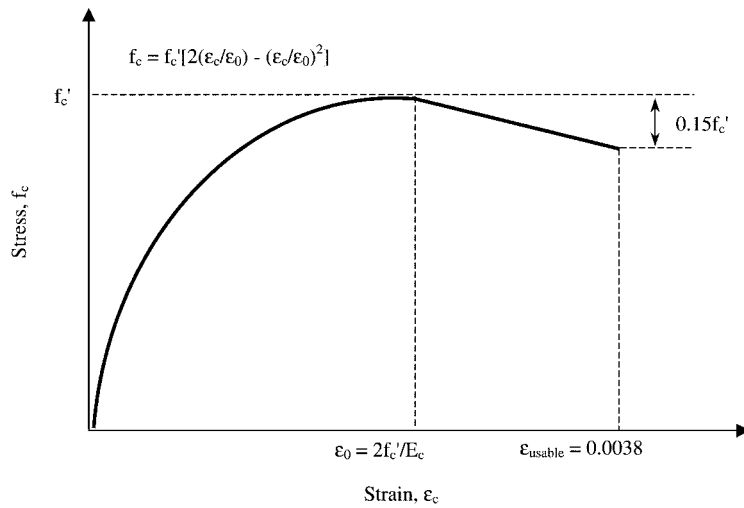
Table 1 Details of experimental test specimens

Group	Beam ID	Tension steel reinforcement	Actual f_y , ksi (MPa)	Stirrup spacing, in (mm)	No. of longitudinal CFRP layers	No. of diagonal CFRP layers	Comments	
1	B1				0	0	Reference	
	B2	2#6	65 (448)	4 (101.6)	1	0	Strengthened	
	B3				1	1	Strengthened <i>w /</i> anchors	
	B1R				1	0	Repaired	
B4	2#4				66(455)	1	0	
2	B5	2#5	68(487)	4 (101.6)	1	0	Strengthened and tensile reinforcement ratio	
	B7	2#7	71(490)		1	0		
	B8	2#8	68(487)		1	0		
	TBA1	2#5	50(345)		6 (152.4)	1		0
TBA3	79(545)		1	1				
TBB1	74(510)		1	0				
TBB2	65(448)		1	1				
4	TBB1	2#5	74(510)	12 (304.8)	1	0	Strengthened and number of layers of CFRP sheet <i>w / o</i> or <i>w /</i> anchors	
	TBB2		65(448)		1	1		
	TBB3		64(441)		12 (304.8)	2		0
	TBB4					2		1
	TBB5					3		0
	TBB6					3		3

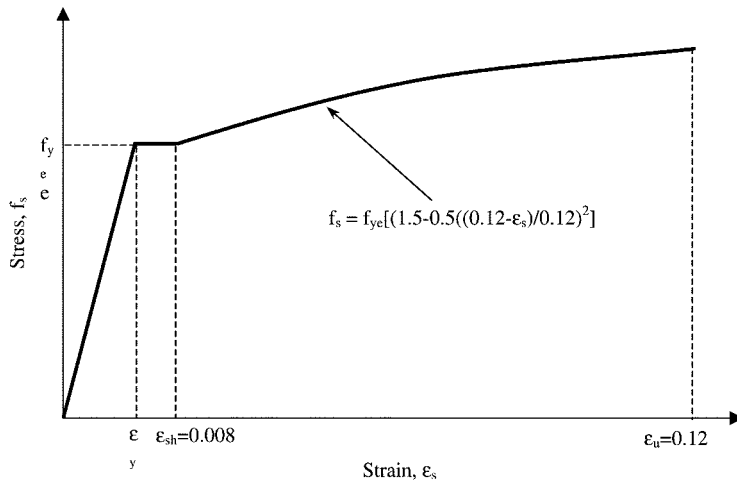
Table 2 Properties of CFRP composites

No. of layers of CFRP composite sheet	Average tensile strength, ksi (MPa)	Tensile modulus, ksi (MPa)	Rupture strain
1*	550 (3792)	33400 (230293)	0.017
1	750 (5171)	39000 (268905)	0.019
2	450 (3103)	37000 (255115)	0.012
3	400 (2758)	35000 (241325)	0.011

* Provided by a manufacturer



(a) Stress-strain relationship for concrete



(b) Stress-strain relationship for steel

Fig. 2 Stress-strain properties for concrete and steel

4.2. Details of the finite elements

4.2.1. SOLID65 element for concrete

A solid element, SOLID65, was used to model the concrete. The solid element had eight nodes, with three degrees of freedom at each node: translations in, x , y , and z directions. The solid element was capable of cracking in three orthogonal directions, crushing of the concrete, plastic deformation, and creep. The compressive stress-strain relationship of the concrete was modeled using a multi-step linear function based on the modified Hognestad's model.

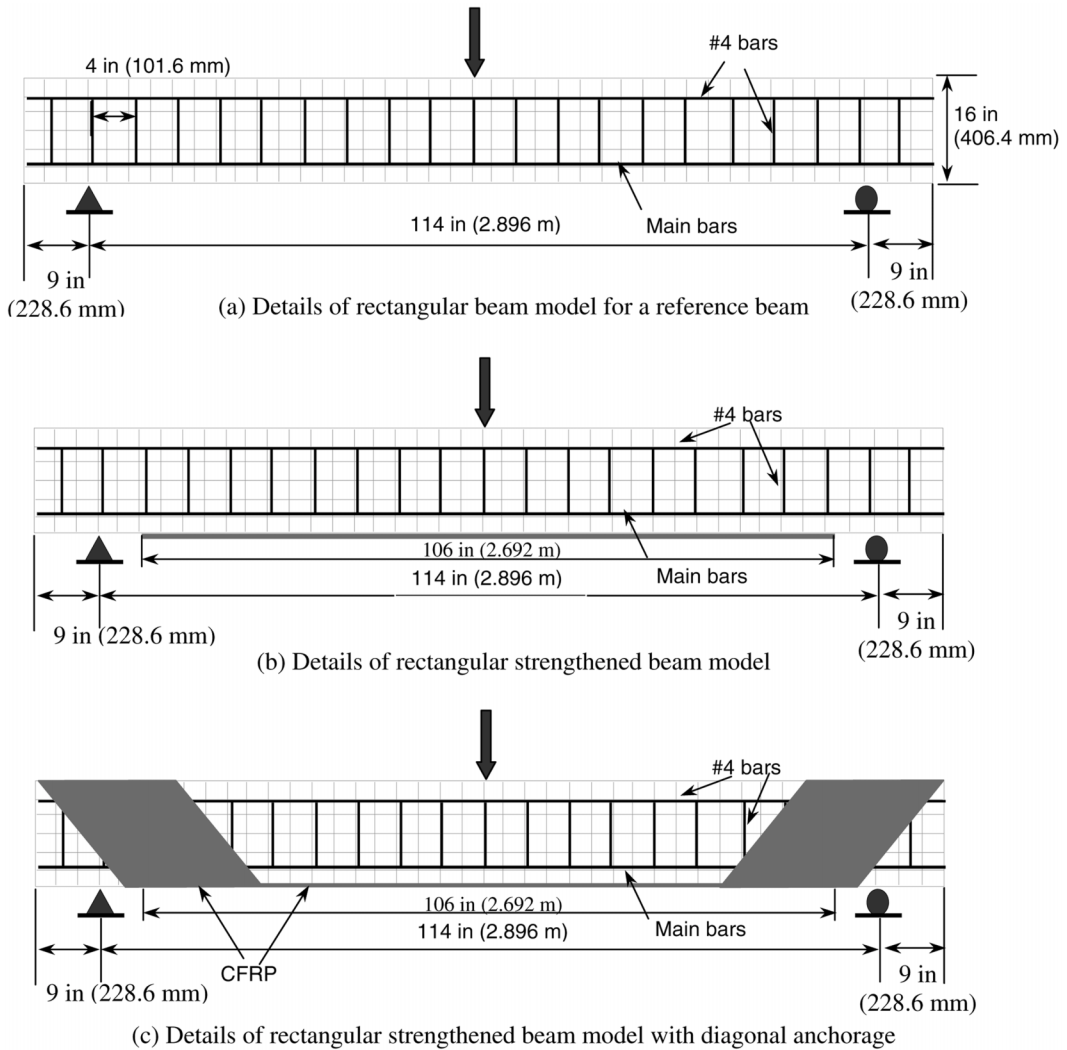


Fig. 3 FEA modeling of rectangular beams

4.2.2. LINK8 element for steel

A link element, LINK8, was used to model the steel reinforcement. The link element was capable of modeling uniaxial tension, compression, and plastic deformation at each node with the same degrees of freedom as the SOLID65 element. The tensile stress-strain relationship of the steel used was modeled using a multi-step linear function.

4.2.3. SHELL63 element for CFRP composites

A shell element, SHELL63, was used to model the CFRP sheets. The shell element had the capabilities of bending, membrane action, stress stiffening, and large deflections at each node with

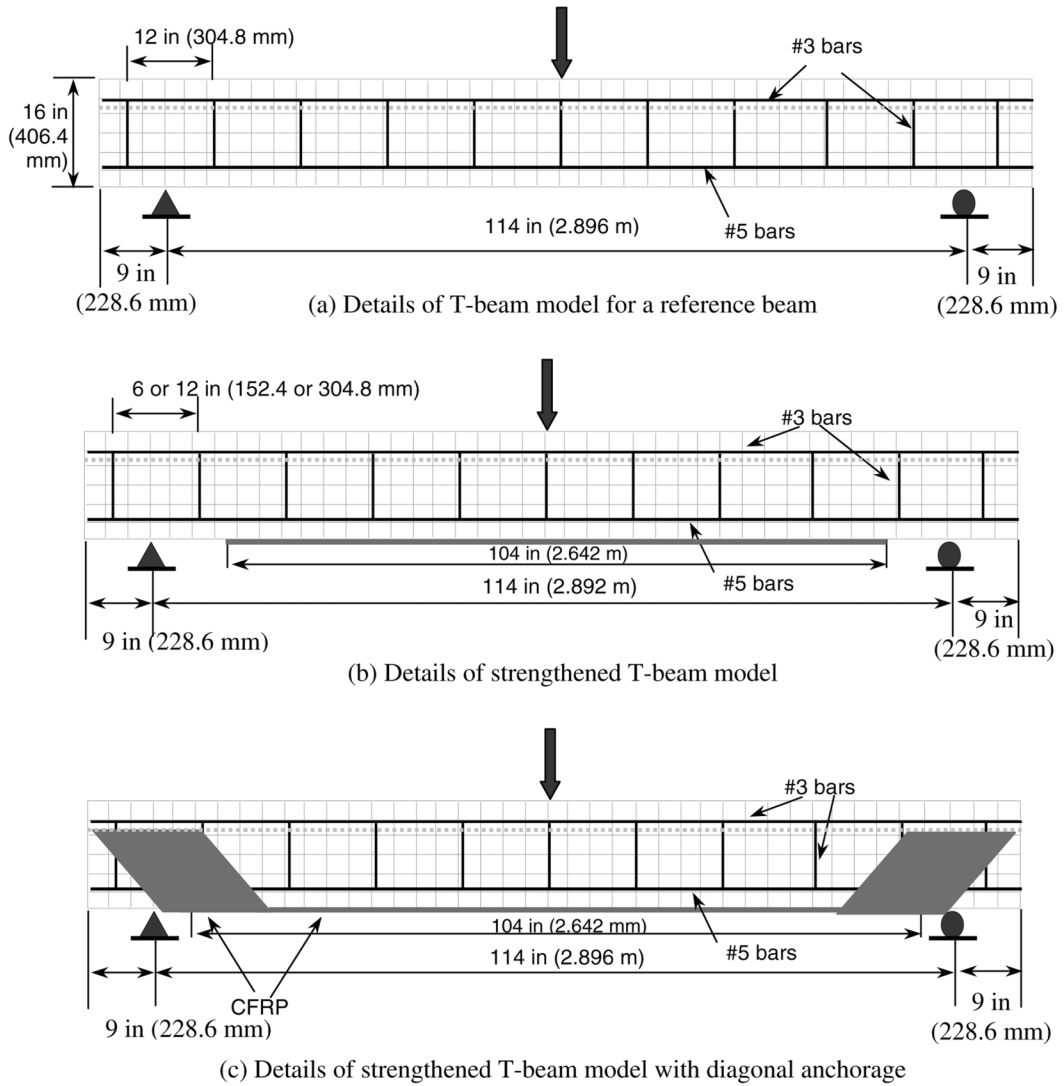


Fig. 4 FEA modeling of T-beams

six degrees of freedom at each node: three for translation and three for rotation. The stress-strain relationship of the CFRP sheets used was linear. The rotational degrees of freedom were fixed for the FEA analysis. The CFRP diagonal anchors were modeled of shell elements, as the longitudinal CFRP sheets.

4.2.4. CONTA173 and TARGE170 elements for contact bond

The non-perfect bonding model requires bonding elements. The bonding elements that were used for the interface between the concrete surface and the CFRP sheet were 3-D contact and target elements, CONTA173 and TARGE170, respectively. The contact element allowed for contact and sliding between the target and deformable surfaces. The target element had a 3-D target surface for

the corresponding contact element. The contact element had three translation degrees of freedom in the x , y , and z directions at each node. The contact element had a capability of contacting on the 3-D solid and shell elements without mid-side nodes, so that it could interact with element, Solid65 and Shell63. The contact element also allowed the modeling of Coulomb and shear stress friction. Target elements made the target surface discretized and associated with the contact surface. An input for the contact element is the contact normal stiffness (KN); a default value of KN is not supplied by ANSYS. KN should be large enough to prevent over-penetration. KN can be estimated by the following equation provided by ANSYS User Manual:

$$KN \approx fEh \quad (1)$$

Where:

f = Factor that controls contact compatibility between two different element surfaces

E = Elastic modulus (if two different materials are used, the smaller value of E should be chosen)

H = Characteristic contact length (should be a contact target length or a typical element size)

The contact element also requires an input for the maximum equivalent shear stress (TAUMAX) for sliding. The default value is 1.0E2.0 ksi (1.5E1.9 MPa), and a reasonable upper limit for TAUMAX is $\sigma_y/\sqrt{3}$, which is the Von Mises yield stress of the surface material given by ANSYS. However, it is believed that empirical data would greatly benefit the model.

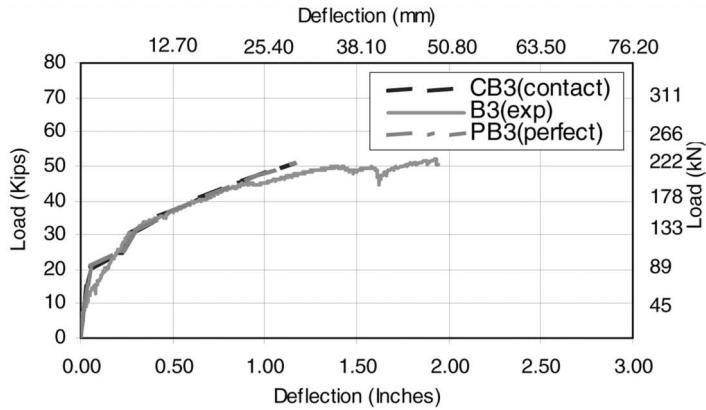
The file naming convention used in the FEA of the perfect bonding models was named using a prefix “P” followed by the name of the experimental beam, for example, PB3 and PTBB1. The file naming convention used in the FEA of the non-perfect (contact) bonding models was named using a prefix “C” followed by the name of the experimental beam, for example, CB2 and CTBB5.

5. Comparison of experimental and FEA results

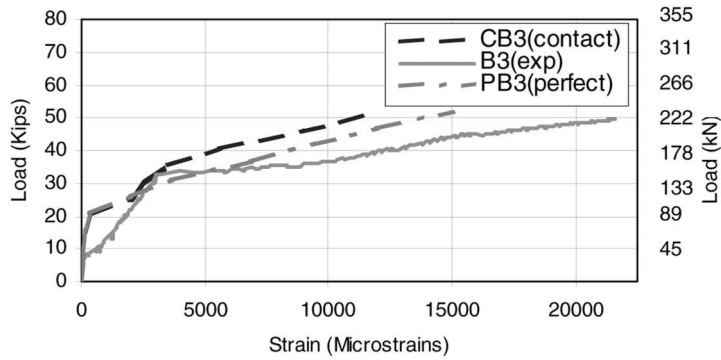
5.1. Load-deformation relationship

5.1.1. Rectangular beam case: Beam B3

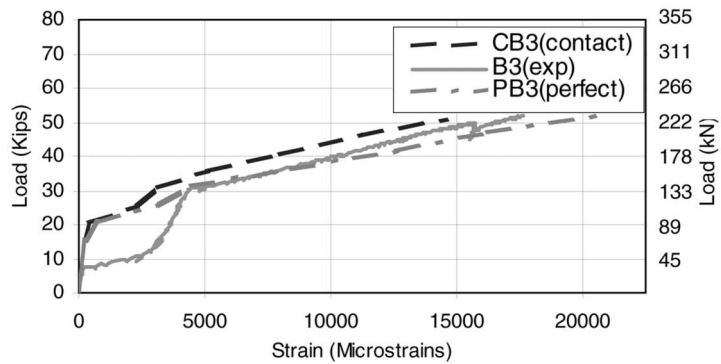
The experimental and FEA load-deflection curves for beams B3, CB3, and PB3 in Group 1 are shown in Fig. 5(a). The FEA failure loads were 51 kips (226.8 kN) and 52 kips (231.3 kN) for the contact bonding model (CB3) and the perfect bonding model (PB3), respectively, as compared to 51.5 kips (229.1 kN) for the experimental results (B3). The corresponding FEA mid-span deflections were 1.16 in. (29.46 mm) and 1.23 in. (31.24 mm) for the contact and perfect bonding models, respectively, as compared to 1.93 in. (49.02 mm) for the experimental results. The experimental and FEA load- tensile steel bar strain curves and load-CFRP strain curves for beams B3, PB3, and CB3 in Group 1 are shown in Figs. 5(b) and 5(c), respectively. The FEA mid-span tensile steel bar strains at failure were 0.0116 and 0.0150 for the contact and perfect bonding models (CB3 and PB3), respectively, as compared to 0.0219 for the experimental results. The FEA mid-span CFRP strains at failure were 0.0146 and 0.0206 for the contact and perfect bonding models (CB3 and PB3), respectively, as compared to 0.0176 for the experimental results. The FEA failure loads showed good agreement with the experimental results. However, the FEA results for deflection at failure were 40% less for the contact bonding model and 36% less for the perfect



(a) Load- deflection curves for B3, PB3, and CB3



(b) Load- tensile steel bar strain curves for B3, PB3, and CB3



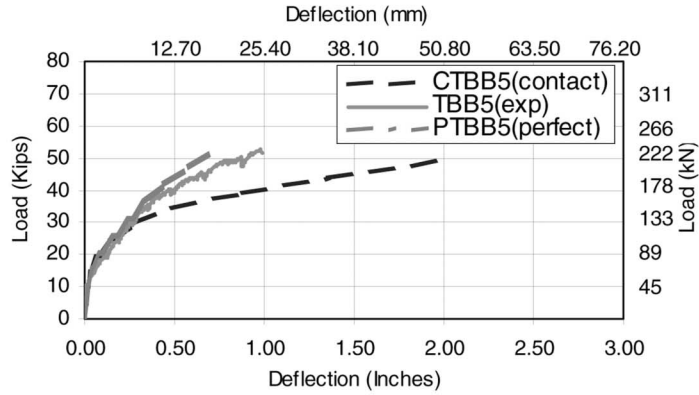
(c) Load-CFRP strain curves for B3, PB3, and CB3

Fig. 5 Comparison of experimental and FEA results (B3, PB3, and CB3)

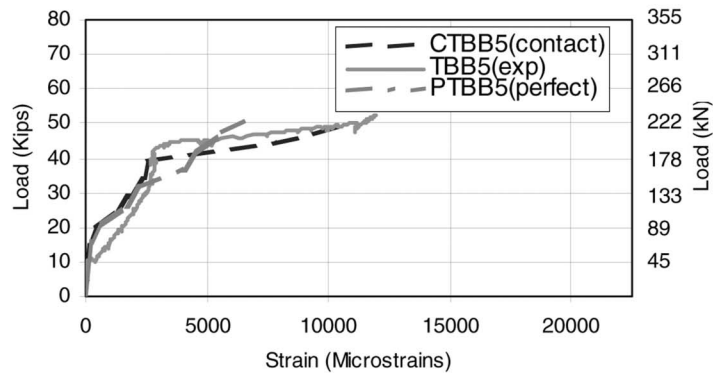
bonding model than that of the experimental results. The FEA results for the tensile steel bar strain at failure were 47% less for the contact bonding model and 32% less for the perfect bonding model than that of the experimental results. The FEA results for the CFRP strain at failure were 17% less for the contact bonding model and 17% greater for the perfect bonding model than that of the experimental results.

5.1.2. T-beam case: Beam TBB5

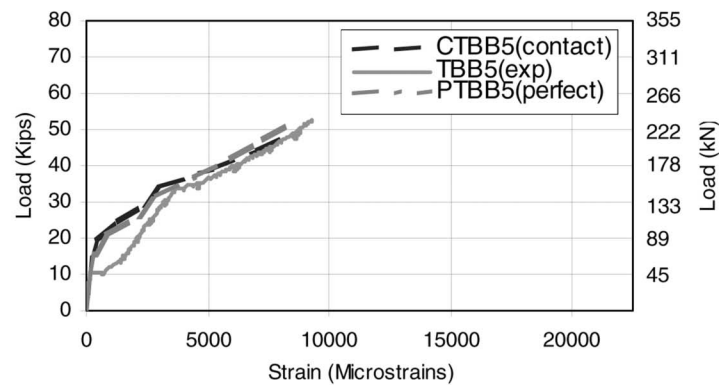
The experimental and FEA load-deflection curves of beams TBB5, CTBB5, and PTBB5 in Group 4 are shown in Fig. 6(a). The FEA results for failure loads were 52.5 kips (233.5 kN) and 49 kips



(a) Load- deflection curves for TBB5, PTBB5, and CTBB5)



(b) Load- tensile steel bar strain curves for TBB5, PTBB5, and CTBB5



(c) Load-CFRP strain curves for TBB5, PTBB5, and CTBB5

Fig. 6 Comparison of experimental and FEA results (TBB5, PTBB5, and CTBB5)

(218.0 kN) for the contact and perfect bonding models (CTBB5 and PTBB5), respectively, as compared to 52.2 kips (232.2 kN) for the experimental results (TBB5). The corresponding FEA mid-span deflections were 1.99 in. (50.55 mm) and 0.73 in. (18.54 mm) for the contact and perfect bonding models (CTBB5 and PTBB5), respectively, as compared to 0.98 in. (24.89 mm) for the experimental results. The experimental and FEA load-tensile steel bar strain curves, and load-CFRP strain curves for beams TBB5, CTBB5, and PTBB5 in Group 4 are shown in Figs. 6(b) and 6(c), respectively. The FEA mid-span tensile steel bar strains at failure were 0.0106 and 0.0070 for the contact and perfect bonding models (CTBB5 and PTBB5), respectively, as compared to 0.0119 for the experimental results. The FEA mid-span CFRP strains at failure were 0.0085 and 0.0086 for the contact and perfect bonding models (CTBB5 and PTBB5), respectively, as compared to 0.0093 for the experimental results. The FEA results for failure load were 0.6% greater for the contact bonding model and 6% less for the perfect bonding model than that of the experimental results. However, the FEA results for deflection at failure were 102% greater for the contact bonding models and 26% less for the perfect bonding model than that of the experimental results. The FEA results for the tensile steel bar strain were 11% less for the contact bonding model and 41% less for the perfect bonding model than that of the experimental results. The FEA results for the CFRP strains at failure were 8.6% less for the contact bonding model and 7.5% less for the perfect bonding model than that of the experiment results.

5.1.3. Overall comparison at ultimate load

Table 3 gives an overall comparison of the experimental, FEA, and ACI results at the ultimate load. The FEA results are in good agreement with those of the experimental results. The results of the FEA perfect and non-perfect (contact) bonding models differ by 1% to 7% from the experimental results. However, compared with the experimental test results, the ultimate load values calculated based on the ACI 440 equations differ by up to 22 %, and some of the results were on the un-conservative side. Based on the analyses presented in this paper, it is believed that the ACI 440 equations should be made more conservative by being calibrated with the experimental tests and FEA models.

5.2. Failure modes

The failure modes of the FEA models were in good agreement with those of the experimental beams. As shown in Fig. 7(a), the flexural-shear cracks in B3 initiated the separation of the CFRP reinforcement from the concrete surface, and then crushing of concrete occurred in the compression zone. Finally, the beam failed by rupture of the CFRP reinforcement on the tension side. As shown in Fig. 7(b), the crack patterns of PB3 (perfect bonding model of B3) were vertical, horizontal, and lateral on the web. Shear-compression cracks in the compression zone on the flange were opened. These FEA crack patterns are very similar to the crack patterns of B3, except for rupture of the longitudinal CFRP reinforcement of the beam.

As shown in Fig. 8(a), the flexural-shear cracks in TBB5 initiated the separation of the CFRP reinforcement from the concrete surface, and then crushing of concrete occurred in the compression zone. Finally, the beam failed by separation of the portion of concrete from the internal reinforcement. As shown in Fig. 8(b), the crack patterns of CTBB5 (contact bonding model of TBB5) were vertical, horizontal, and lateral on the web. At the ultimate load, the flexural cracks

Table 3 Comparison of experimental and analytical results

Group	Beam ID	Experiment		FEA (Finite Element Analyses)				ACI		Comparison		
		Ultimate, P_u , kips (kN)	Ultimate, P_u , kips (kN)	Ultimate, P_{pu} , kips (kN)	Ultimate, P_{pu} , kips (kN)	Ultimate, P_{cu} , kips (kN)	Ultimate, P_{cu} , kips (kN)	Ultimate, P_{aci} , kips (kN)	Ultimate, P_{aci} , kips (kN)	P_u/P_{pu}	P_u/P_{cu}	P_u/P_{aci}
1	B1	32.3	143.7	31.3	139.0	31.3	139.0	29.0	129.0	1.03	1.03	1.11
	B2	45.5	202.4	46.0	204.6	46.0	204.6	43.5	193.5	0.99	0.99	1.05
	B3	52.1	231.7	52.0	231.3	51.0	226.8	43.5	193.5	1.00	1.02	1.20
	B1R	52.5	233.5	N/A	N/A	N/A	N/A	43.5	193.5	N/A	N/A	1.21
2	B4	29.2	129.9	29.0	129.0	29.0	129.0	30.3	134.8	1.01	1.01	0.96
	B5	36.0	160.1	36.0	160.1	36.0	160.1	37.1	165.0	1.00	1.00	0.97
	B7	52.0	231.3	52.0	231.3	52.0	231.3	52.5	233.5	1.00	1.00	0.99
	B8	60.0	266.9	59.5	264.7	60.0	266.9	62.7	278.9	1.01	1.00	0.96
3	TBA1	30.1	133.9	30.0	133.4	29.5	131.2	32.6	145.0	1.00	1.02	0.92
	TBA2	46.8	208.2	47.0	209.1	47.0	209.1	41.4	184.1	1.00	1.00	1.13
	TBB1	40.3	179.3	40.0	177.9	40.0	177.9	40.2	178.8	1.01	1.01	1.00
	TBB2	42.9	190.8	43.0	191.3	43.0	191.3	37.3	165.9	1.00	1.00	1.15
4	TBB1	40.3	179.3	40.0	177.9	40.0	177.9	40.2	178.8	1.01	1.01	1.00
	TBB2	42.9	190.8	43.0	191.3	43.0	191.3	37.3	165.9	1.00	1.00	1.15
	TBB3	48.6	216.2	49.0	218.0	48.0	213.5	52.0	231.3	0.99	1.01	0.93
	TBB4	63.0	280.2	61.0	271.3	60.0	266.9	52.0	231.3	1.03	1.05	1.21
	TBB5	52.6	234.0	52.5	233.5	49.0	218.0	67.8	301.6	1.00	1.07	0.78
	TBB6	79.0	351.4	79.0	351.4	79.0	351.4	67.8	301.6	1.00	1.00	1.17

P_u : Ultimate load of experimental tests

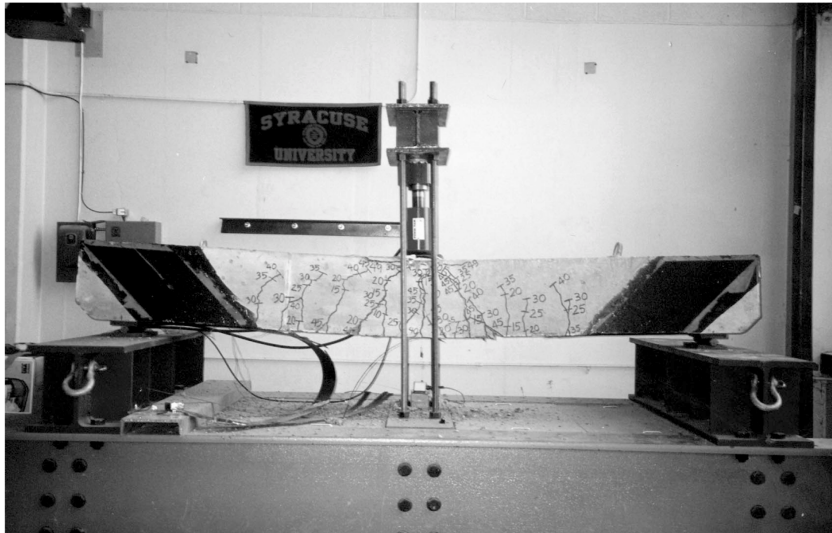
P_{pu} : Ultimate load of FEA analysis with the perfect bonding model

P_{cu} : Ultimate load of FEA analysis with the non-perfect (contact) bonding model

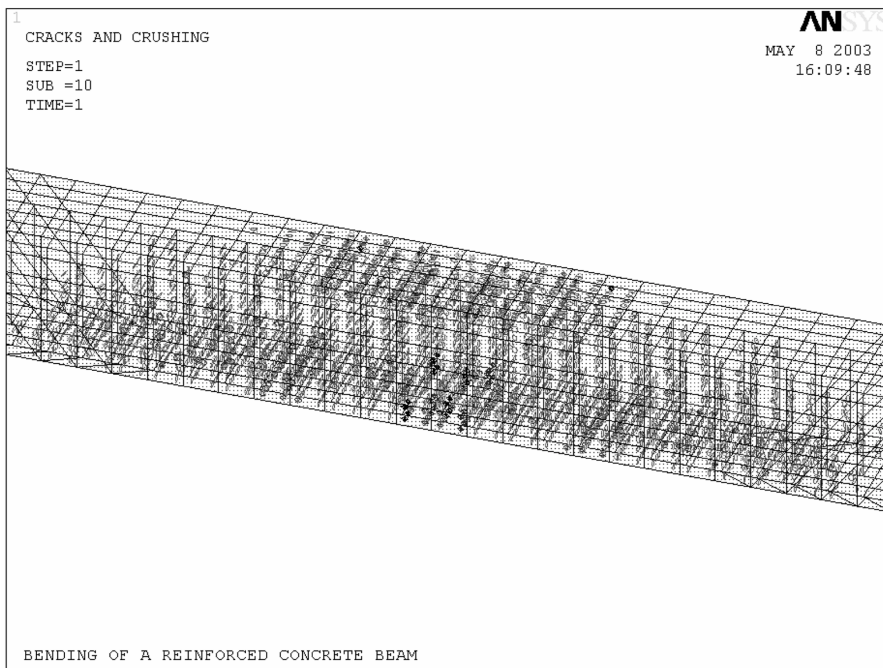
P_{aci} : Ultimate load of ACI

turned into flexural-shear cracks leading to a shear-compression failure of the concrete compression zone. These FEA crack patterns are roughly similar to the crack patterns of TBB5. As shown in Fig. 9, the sliding of the CFRP element from the concrete surface occurred at a distance of 20 in (508 mm) from the center of the beam. That location is similar to the location of initiation of separation of the CFRP reinforcement in TBB5.

Comparing the response of concrete beams strengthened with only longitudinal CFRP sheets, and those strengthened with both longitudinal CFRP sheets and diagonal CFRP anchors, it was very clear that the CFRP diagonal anchors prevented the separation of the longitudinal CFRP sheets, increased beam ductility, and allowed development of the full strength of the longitudinal CFRP sheets.

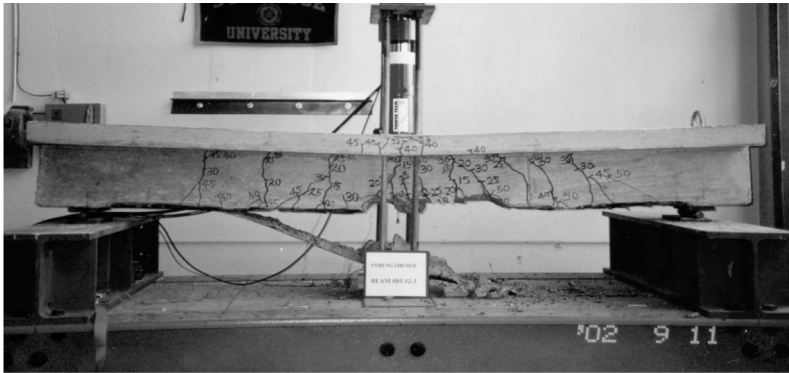


(a) Experimental failure modes for B3

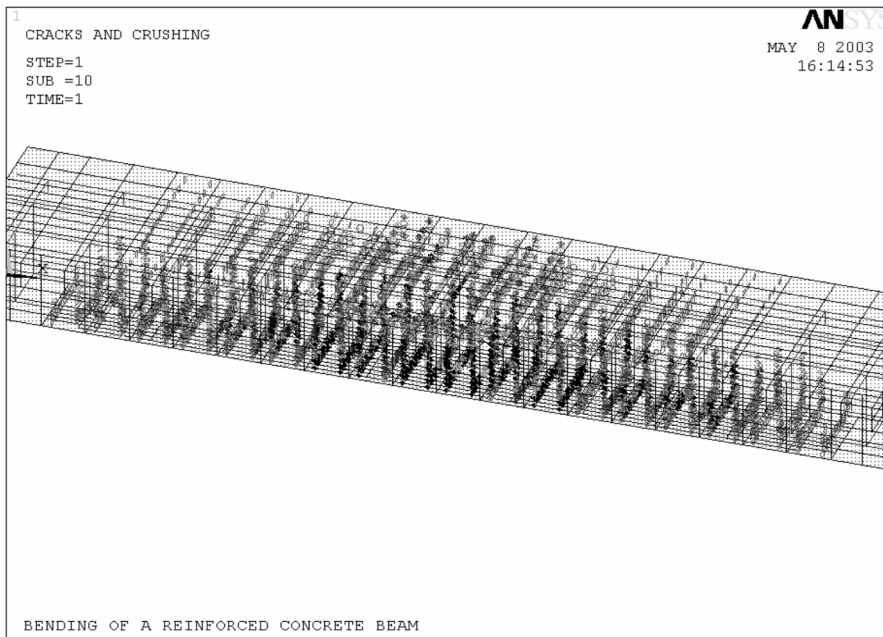


(b) FEA failure modes for PB3

Fig. 7 Comparison of experimental and FEA failure modes (B3 and PB3)



(a) Experimental failure modes for TBB5



(b) FEA failure modes for CTBB5

Fig. 8 Comparison of experimental and FEA failure modes (TBB5 and CTBB5)

6. Conclusions

The response of concrete beam strengthened with longitudinal CFRP sheets externally bonded to the tension side of the beam was investigated under a three-point quasi-static loading. Some of the test beams were also strengthened with additional CFRP diagonal anchors for increased flexural ductility. FEA models were constructed and analyzed. In general, the FEA model did a very good job at predicting test beam's experimental strength, however, it was not as successful in predicting the stiffness and deformations. Further work on enhanced bond models should be explored.

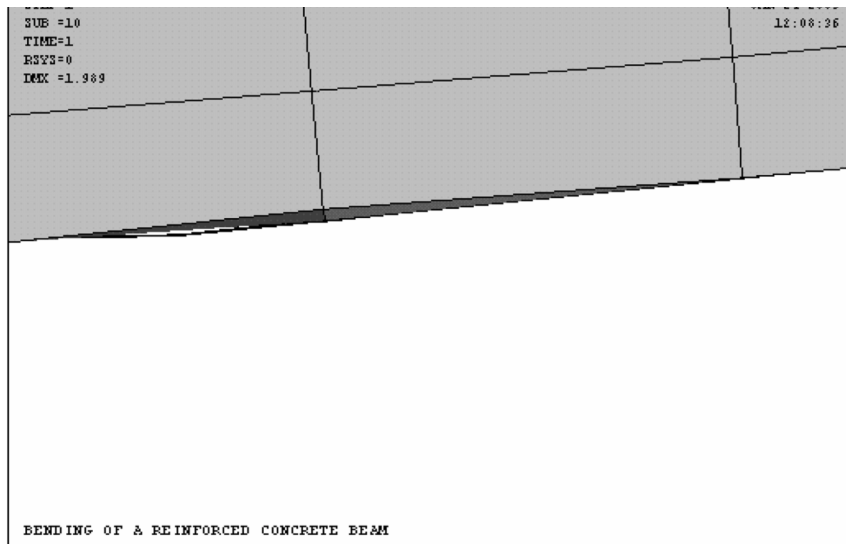


Fig. 9 Sliding of CFRP elements from the surface of the concrete elements for FEA Beam CTBB5

According to the FEA models presented in this paper, the following conclusions could be drawn:

- (1) In general, the FEA is a reliable technique for predicting the response of CFRP strengthened concrete beams. A good bond model is critical for predicting beam stiffness and deformation at failure.
- (2) To determine the flexural strength of the strengthened beams, the use of the FEA model is recommended.
- (3) When the ultimate mode of failure is of concern, a contact element between the concrete and CFRP sheet should be used.
- (4) The use of CFRP diagonal anchors prevents the separation of the longitudinal CFRP sheets, increase beam ductility, and allow development of the full strength of the longitudinal CFRP sheets bonded to the tension side of the concrete beam.

Acknowledgements

The authors gratefully acknowledge the financial support provided by the Federal Highway Administration (FHWA) and the New York State Department of Transportation (NYDOT). The donation of the Replark CFRP system and the technical support provided by the Sumitomo Corporation of America is also gratefully acknowledged.

Conversion factors

- 1 in. = 25.4 mm
- 1 kip = 4.448 kN
- 1 ksi = 6.895 MPa

References

- Ross, C. A., Jerome, D. M., Tedesco, J. W., and Hughes, M. L. (1999), "Strengthening of reinforced concrete beams with externally bonded composite laminates", *ACI Struct. J.*, March-April, 212-220.
- Wong, Rita S. Y., and Vecchio, Frank J. (2003), "Towards modeling of reinforced concrete members with externally bonded fiber-reinforced polymer composites", *ACI Struct. J.*, Jan.-Feb., 47-55.
- Kachlakev D. I. (2002), "Finite element analysis and model validation of shear deficient reinforced concrete beams strengthened with GFRP laminates", *Third Int. Conf. on Composites in Infrastructure ICCI02* June, 1-11.
- ACI Committee 440 Report (2000), "Guide for the design and construction of externally bonded frp systems for strengthening concrete structures", (Revised 24 May 2000). American Concrete Institute, Farming Hills, Michigan, 1-89.
- ANSYS-Release 5.7 (2002), a Finite Element Program for Nonlinear Structural Analysis and User Manual, ANSYS Inc.

CC